Aerospace Science and Technology 145 (2024) 108870

Contents lists available at ScienceDirect

Aerospace Science and Technology

journal homepage: www.elsevier.com/locate/aescte

Optimal design of a clamp band system based on genetic algorithm and experimental verification

Baoshi Yu [a,b], Dapeng Zhang [a,b], Xinfeng Wu [c], Sondipon Adhikari [d], Yongjun Lei [a,b,*]

[a] College of Aerospace Science and Engineering, National University of Defense Technology, Changsha 410073, China
[b] Hunan Key Laboratory of Intelligent Planning and Simulation for Aerospace Mission, Changsha 410073, China
[c] China Astronaut Research and Training Center, Beijing 100094, China
[d] James Watt School of Engineering, The University of Glasgow, Glasgow G12 8QQ, UK

ARTICLE INFO

Communicated by Dr Pinqi Xia.

Keywords:
Clamp band system
Parameterized modeling method
Genetic algorithm
Optimal design
Explicit nonlinear analysis
Separation shock

ABSTRACT

As one of the most common separation systems, the clamp band system (CBS) is widely used in the process of connection and release of spacecraft with the launch vehicle. An optimal design method and a separation shock response estimation method were proposed for a large-diameter CBS in this paper. First, a new application based on the parameter modeling method of MSC.Patran and genetic algorithm (GA) was proposed to design the CBS. Finite element techniques for 2D axisymmetric analysis of the CBS were developed, including the modeling of V-clamp, strap pre-tension, and loads, then the optimizing constraints and objectives were also defined. Secondly, a CBS with a diameter of 3 m was designed via the proposed method, which is verified by the 3D finite element analysis under MSC.Marc and a stiffness experiment. Thirdly, the separation process of the CBS and its high-frequency and high-amplitude shock response were calculated by an explicit dynamic solver, and the differences between the model and experimental results were discussed. Finally, a single degree of freedom (SDOF) spring-mass system was constructed to predict the weakening effect of the delay time on the shock response. The slow-release device was designed and the experiment was completed to verify the effectiveness of the method.

Introduction

The clamp band system (CBS) is one of the most popular separation systems and is widely used in the process of connection and release of the spacecraft with the launch vehicle [1–2]. In the launch phase, the CBS mainly bears the axial load and maintains the stable connection of the satellite. In the phase of satellite separation, the dynamic envelope of the clamp band and separation shock responses also have significant effects on the attitude of the satellite. Therefore, the bearing characteristics of CBS largely determine the success of space launch missions. The complex contact of multiple components and heavy loading conditions in CBS result in nonlinear behavior. Based on this, it is difficult to establish a CBS calculation model that accurately tracks mechanical behavior and carries out corresponding experimental research.

Even so far, the engineering experience of proven designs is the main designing tool [3–4]. In another way, a large number of simulations and experimental research have been carried out to study the complicated mechanical characteristics and behavior of the CBS [5–7]. Robert et al. [5] first combined the nonlinear finite element method with experiments to establish a two-dimensional finite element model of the CBS. Subsequently, Rome et al. [8] introduced two computational techniques for determining the structural capability of the CBS and investigated the effects of physical parameters on the structural capability using 3D finite element models. Singaravelu et al. [9] presented a methodology for the evaluation of the proof load factor for the CBS and established an empirical relation for the failure load in terms of the structural ultimate strength, geometric parameters, and crack defects. Barrans et al. [10–11] studied the bearing capacity of torque, ultimate axial bearing capacity, and distribution of contact force of V-section band clamps by the finite element method.

Among them, the research on experiments is difficult to adapt to the increasing variety of launch tasks due to the high cost, especially for unlocking and separation. Therefore, the research on simplified modeling estimation and system simulation calculation of the dynamic performance of CBS has become a hot topic. Takeuchi and Onoda [12] proposed a free vibration model to simplify the satellite separation impact. Iwasa et al. [6] estimated the separation shock for the V-band clamp separation device based on a single degree of freedom (SDOF) system. Tan et al. [13] simplified the separation of interface rings by an axisymmetric circular ring vibration model, and analyzed the influence

* Corresponding author.

https://doi.org/10.1016/j.ast.2024.108870
Received 9 November 2023; Received in revised form 12 December 2023; Accepted 3 January 2024
Available online 7 January 2024

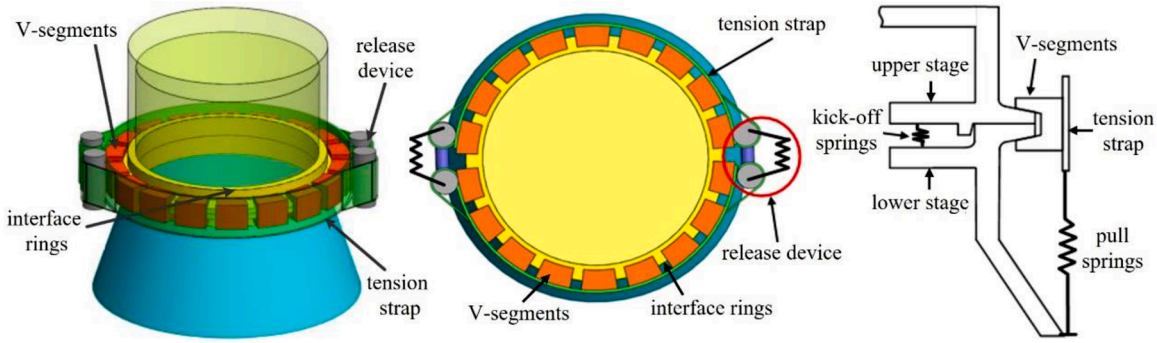

Fig. 1. The configuration of a clamp band system.

of main geometric parameters on shock response, but the verification was only through the finite element method rather than experiment compared with previous studies. For the complex separation process and high shock response of large-diameter CBS, the analysis methods and corresponding impact reduction methods need to be further studied.

Recently, Qin et al. [14–16] have done a lot of research on the modeling and analysis of the clamp band system. Through the nonlinear finite element analysis method, the modal parameter identification and axial tensile bearing characteristics analysis of the CBS are completed. Combined with the static experiment of the proportional model, the correctness of the nonlinear finite element analysis is verified [17–18]. In addition, Qin and Yan also developed an analytical model for the bending stiffness of the clamp band joint which was validated by finite element analysis. Based on the analytical model, the bending behavior of the clamp band joint was studied [2]. The above research gives some examples of the CBS 3D finite element model, which not only realizes accurate characteristic analysis but also brings the problems of model convergence and high-cost calculation to researchers. This problem will be more serious in optimization design.

A more efficient 2D finite element model was proposed to study the dynamics of clamp band connection structures under longitudinal substrate excitation, and the reliability is demonstrated by 3D model comparison. The inaccuracy of the 2D model in nonlinear friction behavior simulation is compensated with quasi-static test data [19]. However, it is difficult to apply the updated model based on experimental data in optimized cluster computing. A surrogate model technique, which can approximate time-consuming simulation / experimental models into low-cost digital models, is widely used in complex engineering system optimization [20–22]. Based on the surrogate model, the rapid prediction of structural performance can be realized, and the model has good algorithm adaptability. Applied to the optimization of CBSs, Wang et al. [23] analyzed the influence of key parameters on load-bearing and separation performance and then optimized the structural dimensions of the CBS via Kriging surrogate model. Considering the multivariable coupling constraint problem in CBS optimization, YU et al. [24] proposed a constrained sequential approximate optimization method to efficiently complete the lightweight design of a CBS. However, the approximate accuracy of the surrogate model requires the number of sample sets when constructing the model. The high-precision and fast-response surrogate model that often meets the performance prediction requirements requires a certain scale of sample points, and its training process also poses a challenge to the computational cost. Using the symmetry of structural configuration and load, simplifying the 3D finite element model into a 2D axisymmetric model can fundamentally save the cost of a single calculation in optimization. When the 2D axisymmetric model is used for optimization, its reliability is crucial to avoid the accumulation of errors. Guo et al. [25] established a 2D axisymmetric model of a rigid clamp band and carried out structural configuration optimization, which effectively improved the overall connection performance. The accuracy of the axisymmetric model was verified by comparing it to the 3D model. It is worth noting that the 2D axisymmetric model established by Guo is for circumferential continuous V-segment, and its equivalent error is unacceptable for most CBS with discrete V-segment. The above studies have given effective CBS design schemes. However, the verification is only through the finite element model, and no experiments are carried out. The persuasion and applicability of the design scheme are limited.

Using metaheuristic algorithms to drive structural optimization has become an efficient structural design method. Compared with the traditional empirical design method, the optimization design combined with the algorithm has higher search efficiency for the overall optimization space. In addition, the designable space dimension is also larger [26]. The above optimization design of CBSs also covers the application of some intelligent algorithms, which proves that intelligence-driven optimization is feasible. The core point lies in the combination of algorithm and model to achieve the balance between accuracy and efficiency. Taj et al. [27] combined multi-objective genetic algorithm and high fidelity Gaussian Process model to optimize aircraft geometries. However, to the best of our knowledge, there are few studies on the application of algorithms and models in CBS design.

Careful consideration of the published literature in the field of structural optimization design, as concisely presented in the preceding paragraph, shows that the optimization method of machine learning-driven by physical mechanism has not been fully researched and applied for CBSs, despite the traditional design method based on experience is inefficient and difficult to generalize. In practice, there is an increasing demand for large-diameter CBS for deep space exploration missions. With the increasing attention to intelligent design in engineering structures, the necessity of design and verification of fusion multi-paradigm have become rather apparent from the viewpoint of effective computational modeling and design framework with high generalization ability. A new approach based on the parameter modeling method of MSC. Patran and genetic algorithm (GA) is proposed to design a large CBS (Radius is 1.5 m) in this paper. Finite element techniques for 2D axisymmetric analysis of a clamp band system are developed, including the modeling of V-clamp, strap pretension, and loads, and the optimizing constraints and objectives are also introduced. Then parametric studies are performed to determine the influence of relevant factors and a 3D finite element model is established to verify the optimized result. Based on the explicit nonlinear analysis method, the study of the separation process and separation shock of the CBS is solved, and the dynamic envelope of the clamp band and separation shock responses are also obtained using LS-DYNA. Then a SDOF 'spring-mass' system is utilized to estimate the shock response during the separation process, and the effect of delay time on the impact reduction is studied. Finally, the full-scale stiffness experiment and separation experiment were carried out to verify the accuracy of the above models.

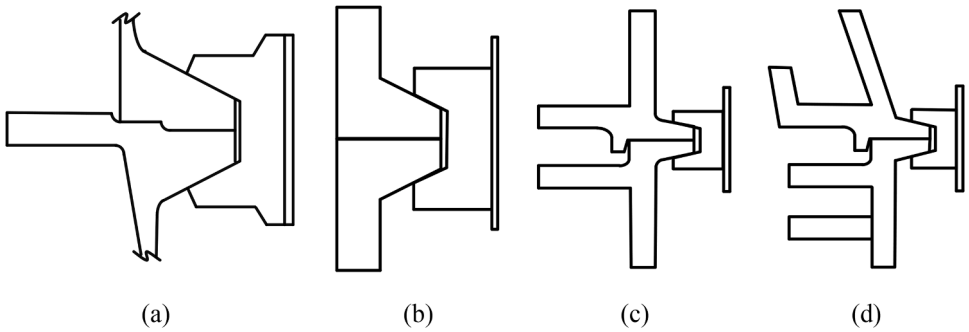

Fig. 2. Four kinds of cross sections of clamp band system.

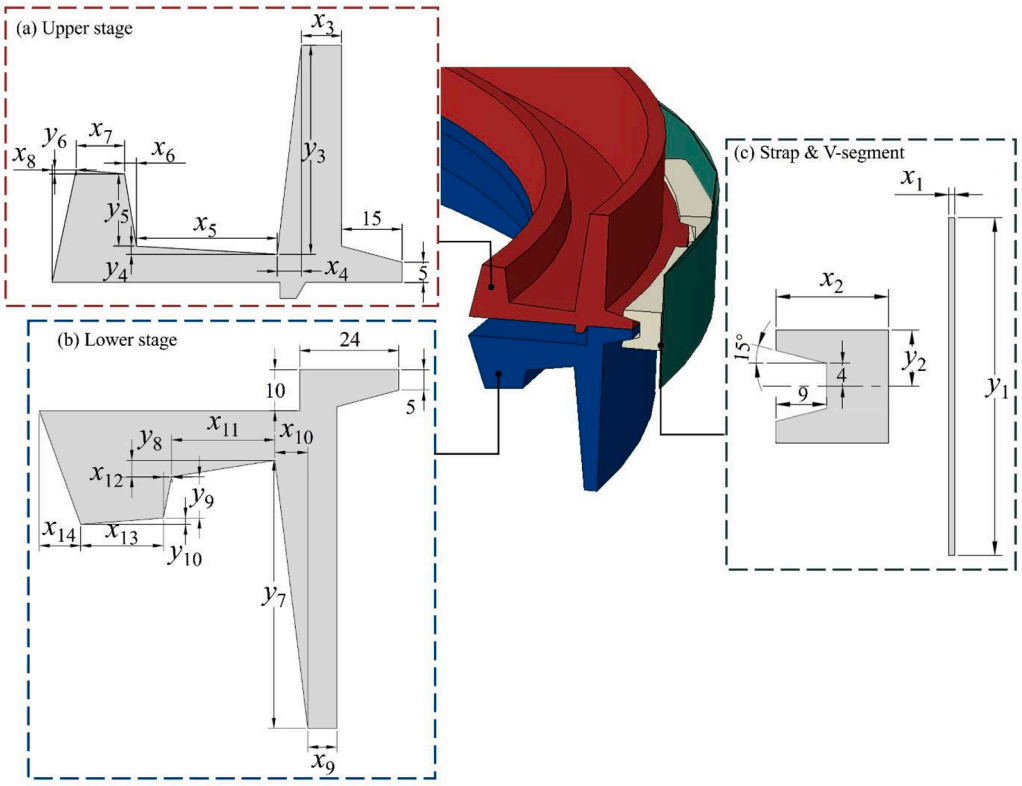

Fig. 3. General configuration of CBS in optimal design.

Optimal design based on axisymmetric model

As shown in Fig. 1, a typical CBS consists of two tension straps, several V-segments, and two release devices (explosion bolts). The tension straps resulted in inward radial force on the V-segments, which fastened the interface rings of the upper stage and lower stage together. When the separation order of spacecraft and launch vehicle is executed, the explosion bolts work and then the interface rings separate. In addition, the kick-off springs of a CBS are usually used to accelerate the process of separation, prevent collision between the lower and upper stages, and pull the released clamp away from the upper stage.

Several items must be considered in the design of CBS [28], including the selection of release devices, friction control, separation dynamics, system strength and stiffness, installation procedures, etc. All of these items are very important for designing a reliable CBS. However, in this paper, more attention is paid to structural strength and stiffness. On the one hand, tension straps and V-segments are the main components of CBS, and they are relatively easy to design. On the other hand, the upper stage and lower stage are taken into account here for their large contribution to the system's strength and stiffness. To increase the local stiffness, especially for interface rings with large radii, the cross-section of interface rings can be designed into various shapes [17] as shown in Fig. 2.

Based on those kinds of interface rings, a general configuration is designed as shown in Fig. 3. In this figure, parameters $x_1 \sim x_{14}$ and $y_1 \sim y_{10}$ can't be obtained by theory analysis and need to be determined through optimal design, and the other parameters are obtained via the experience formulas and proven designs in the former design process. However, the nonlinear factors, such as the gap, friction, and contact between the interfaces, will make the convergence of the calculation difficult in the optimization. So the appropriate optimization method will greatly improve efficiency. A method based on the parameter modeling method of MSC. Patran and GA are proposed as follows.

The flowchart of the proposed optimal design method is shown in Fig. 4. Among them, the parametric modeling language PCL (Patran Command Language) of MSC.Patran and the nonlinear solver MSC.Marc are used to obtain the deformation and stress distribution of the 2D finite element model under different design parameters. Then, GA is used to

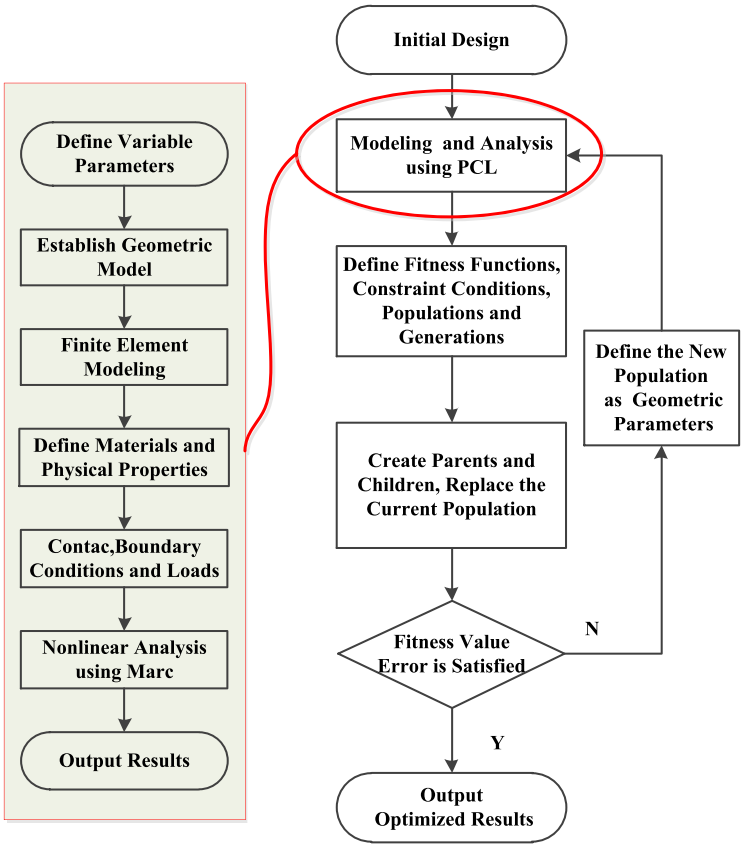

Fig. 4. Design flowchart of clamp band system.

Table 1
Key functions in PCL.

Module	Effect	Function command
Initiate program	Create DB files; define Marc solver	uil_file_new.go uil_pref_analysis. set_analysis_preference
Define parameters	Define real & integer variables	global real global integer
Group	Create a group Set the current group	ga_group_create ga_group_current_set
Establish Part	Form geometric models with points, lines & surfaces	asm_const_grid_xyz asm_const_line_xyz sgm_const_surface_4edge
Mesh	Set node seeds divide surface elements	mesh_seed_create fem_create_mesh_surf_4
Define property	Define material properties & element characteristics	material.create elementprops_create
Load	Define the load & boundary conditions	loadsbcs_create
Extract results	Import results Output to a document	res_data_load_dbresult text_open; text_write; text_close

simulate the biological evolution process, determine the search direction and range, approach the optimization goal, and finally determine the optimization result. The core technologies in the flowchart are PCL and GA.

PCL has almost all the functions of standard C language, and various operations are implemented in PCL in the form of functions. The key functions in modeling and nonlinear analysis are listed in Table 1, including key modules such as defining parameters, setting loads, and dividing elements. The corresponding solver is MSC.Marc, which has powerful nonlinear solving function.

For the optimal design of CBS in this paper, multiple variables and constraints (coupling constraints between variables and performance constraints) lead to high-dimensional and irregular design domain, and conventional gradient algorithms are easy to produce local optima. Although the intelligent algorithms can solve the global optimal solution, it is obviously a more 'expensive' strategy than the gradient algorithm. However, the 2D axisymmetric model is used to accelerate the evaluation of the objective function, which makes the efficiency of the intelligent algorithm based on population information acceptable. Therefore, as a classical metaheuristic algorithm, GA is adopted in this paper. It is a classical algorithm abstracted from the natural evolution process, which is widely used in neighborhood search and optimization problem solving because of its good global exploration ability [29–32].

Axisymmetric finite element modeling

Aiming at the distribution symmetry of the CBS structure, the optimization of the 2D axisymmetric finite element model will greatly reduce the calculation cost. By comparing with the results of 3D finite element and full-scale experiment, the accuracy of the axisymmetric model is verified. Axisymmetric modeling consists of four parts: the

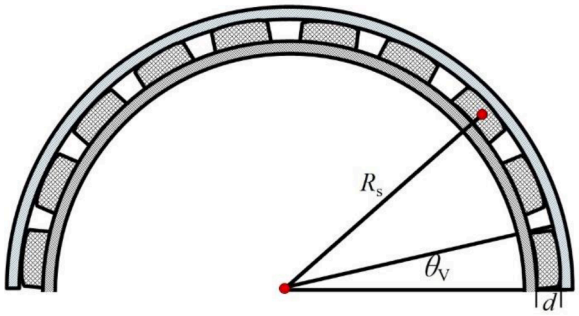

Fig. 5. Distribution of V-segments in the circumferential direction.

creation of mesh, the definition of materials and properties of these elements, the equivalent of pre-tension and loads, and non-linear analysis.

(1) Equivalent modeling of V-segments

Under the assumption that the influence of the joint on the local deformation and stress is neglected, the discrete V-segments are modeled as a continuous structure in the process of establishing a 2D axisymmetric finite element model, in which the material parameters are determined based on equivalent stiffness and mass. In Fig. 5, considering the axial tension stiffness, the V-segments can be simplified as a system of paralleling springs, the stiffness formula is

$$K_T = \sum_{i=1}^{N} K_{Ti} \tag{1}$$

where $K_{Ti} = EA/L$ is the axial tension stiffness of a V-segment, E is the elastic modulus of the V-segment, A is the cross-sectional area of a V-segment, and L is the distance between the axial loads on the V-segment. Moreover, N is the total number of V-segments.

Then the coverage ratio can be defined as

$$\delta = \frac{A_V}{A_{Total}} = \frac{N\theta_V R_s d}{2\pi R_s d} = \frac{N\theta_V}{2\pi} \tag{2}$$

where A_v is the sum of the cross-sectional areas of discrete V-segments, namely $A_v = A\,N$, A_{Total} is the total cross-sectional area after equivalence, R_s is the average radius of the flange, d and θ_v are the equivalent thickness and angle of the V-segment respectively.

The axial stiffness is given by

$$K = \frac{EA_V}{L} = \frac{E\delta A_{\text{Total}}}{L} = \frac{E_{equ}A_{Total}}{L} \tag{3}$$

So the equivalent elastic modulus and density are respectively expressed as

$$\begin{cases} E_{equ} = \delta E \\ \rho_{equ} = \delta \rho \end{cases} \tag{4}$$

The distribution of the strain and deformation of V-segments are accurate based on these formulas [19], but the stress is "average" stress which should be converted to the true stress by $\sigma_{true} = \sigma_{average}/\delta$..

(1) Application of pre-tension

It is important to model the pre-tension in the strap caused by bolt tightening. In general, the tension is generated by the application of a temperature differential in the finite element analysis [8], which can be obtained by

$$\Delta T = \frac{F_{pt}}{E_t A_t \alpha_t} \tag{5}$$

where F_{pt} is the pre-tension, E_t and α are respectively elastic modulus and coefficient of thermal expansion for the strap material, A_t is the area of cross-section of the strap. Considering the per-tension is applied only along the circumferential direction, the coefficient of thermal expansion in the circumferential direction can be defined as a constant value, while the values of the other two directions are set to zero.

$$\begin{cases} \alpha_R = 0 \\ \alpha_T = const \\ \alpha_Z = 0 \end{cases} \tag{6}$$

Since the circumferential contraction of the strap cannot be reflected in the 2D model, it is necessary to complete the application of the pre-tension in the 3D model in the above way. At the same time, the radial contraction displacement of the strap under the corresponding pre-tension is calculated and applied to the 2D model as an equivalent load.

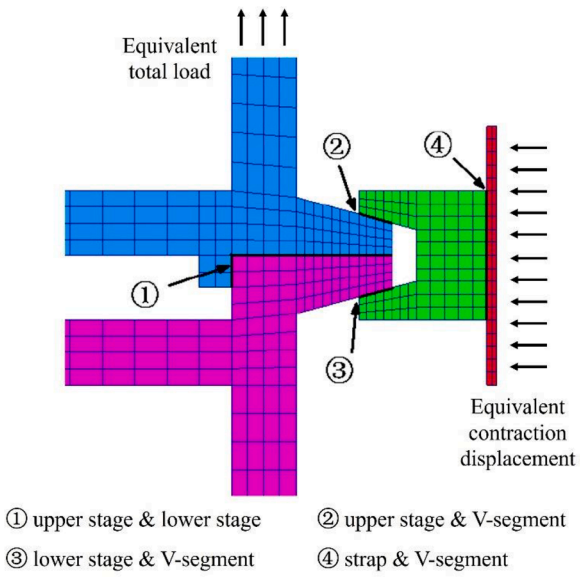

Fig. 6. Load and contact surfaces in 2D axisymmetric models.

(1) Axisymmetric loads

In the axisymmetric analysis, the tension force $_T$, bending moment $_M$, and shear force Q should be converted to axisymmetric loads by the following formulas [8]:

$$\begin{cases} q_T = \dfrac{T}{2\pi R_s} \\ q_M = \dfrac{M}{\pi R_s^2} \\ q_Q = \dfrac{Qh}{\pi R_s^2} \end{cases} \tag{7}$$

where q_T,q_M and q_q are respectively the equivalent axial line force of tension force, bending moment, and shear force. h is the axial distance from the mating rings to the location of the shear load application. The total load is calculated as

$$q_{total} = q_T + q_M + q_Q \tag{8}$$

The equivalent total load q_{total} is applied to the top of the upper stage, while the bottom of the lower stage is fixed constraints.

The contact relationship and load application in the 2D model are shown in Fig. 6. The V-segments have contact surfaces with the straps and the interface rings. There are also contact surface pairs between the interface rings. The Coulomb friction model is applied to simulate the friction of each pair of connected surfaces. 2D solid elements are used, which is suitable for axisymmetric models, and mesh convergence analysis for the 2D model is performed to ensure that the nodes on the contact surface correspond and the mesh density is appropriate.

Optimization problem and contents of the GA

GA includes the process of population selection, crossover, and mutation, and acts on the population by defining the operator. According to the design process shown in Fig. 4, the main steps are to determine the constraint function and the fitness function. The optimization problem and the fitness function are described below.

(1) Formulation of the optimization problem

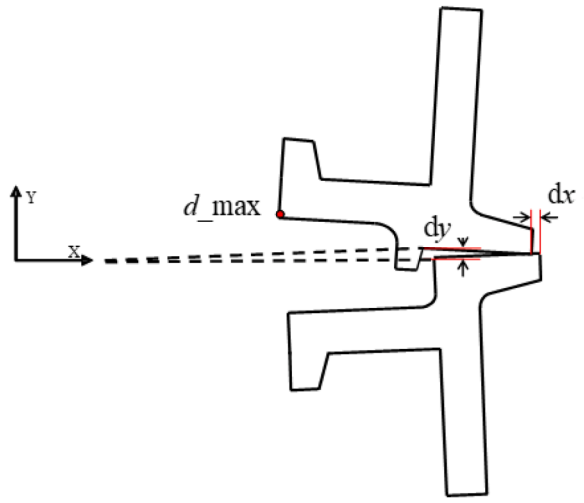

Fig. 7. Deformation of interface rings.

For the optimization of CBS in this paper, the 24 geometric parameters in Fig. 3 are used as design variables, and the minimum structure mass is set as the objective function, while the bearing capacity is regarded as the constraint function. Generally, the constraint function consists of strength constraints and stiffness constraints. The separation dynamic response of CBS is not set in the constraint, but the optimization results are verified by experiments and simulations. However, it is difficult to express the bending stiffness of CBS in the axisymmetric model. In this paper, a whole elastic deformation and a local stiffness are defined to reflect the bending characteristics. For the calculation of the elastic deformation, each component of the CBS is regarded as a whole structure (simplified thin-walled cylinder model). Let's define the minimum bending stiffness of the CBS as

$$K_{b\_\min} = EI = \frac{E\pi\left(R_s^4 - r^4\right)}{4} = \frac{E\pi\left(R_s^4 - \left(R_s - d_{\min}\right)^4\right)}{4} \tag{9}$$

where $K_{b\_\min}$ is the required stiffness, and $d_{\min}$ is the minimum thickness of interface rings. It can be obtained based on $K_{b\_\min}$, then x_3 and x_9 should be bigger than $d_{\min}$.

Next, the local stiffness is constrained by the gap and slip. As shown in Fig. 7, three parameters are defined to constrain the local stiffness. The displacement of the inner ring $d\_\max$ is constrained to avoid large bending deformation. The slip dx is a very small parameter and depicts the slip displacement of the upper stage. The gap dy is obtained by the following formulas:

$$\theta_{gap} = \frac{dy}{R_s} \tag{10}$$

$$C_b = \frac{\theta_{\text{gap}}}{M} = \frac{dy/R_s}{q_M \pi R_s^2} = \frac{dy}{q_M \pi R_s^3} \tag{11}$$

$$dy = C_b q_M \pi R_s^3 \tag{12}$$

where C_b is the flexibility coefficient of the CBS.

In summary, the mathematical expression of the optimization problem can be written as:

Table 2
Parameter setting of GA.

Parameter	Type	Value
Genetic representation	Coordination	
Fitness	Mass & constraints	
Selection	Deterministic	
Chromosome length		24
Population size		60
Termination	Iteration	50
Crossover	One-point crossover	
Crossover-rate		0.9
Mutation-rate		0.05

$$\begin{aligned}
&\text{Find}: \boldsymbol{x} = [x_1, \cdots, x_{14}, y_1, \cdots, y_{10}]^T \\
&\text{Min}: m(\boldsymbol{x}) \\
&\text{S.T.}: \sigma_{\max} < \sigma_s \\
&dy < C_b q_M \pi R_s^3 \\
&dx < dx_{cons} \\
&d_\max < d_\max_{cons} \\
&\boldsymbol{x}_{\min} < \boldsymbol{x} < \boldsymbol{x}_{\max}
\end{aligned} \tag{13}$$

where x is the design variable; $m(\boldsymbol{x})$ denotes the weight of the structure;σ_s is the yield stress, dx_{cons} and $d\_\max_{cons}$ are the maximum slip displacement and the maximum displacement of the inner ring respectively.

(1) Fitness function

The selection of fitness function in a GA directly affects the efficiency of the algorithm and whether the optimal solution can be found. For the optimization problem in this paper, the fitness function takes into account both the objective of lightweight structure and the constraints of static performance (strength and bending stiffness). Then the fitness function is defined as follows:

$$M(\boldsymbol{x}) = m(\boldsymbol{x}) + \sum_{i=1}^{5} \Delta f(x_i) \tag{14}$$

where $\Delta f(x_i)$ represents the five constraints in Eq. (13), and the expression is

$$\Delta f(x_i) = \begin{cases} F(x_i) - f(x_i) iff(x_i) \le F(x_i)_{con} \\ C_i\left(f(x_i) - F(x_i)\right) iff(x_i) > F(x_i)_{con} \end{cases} i = 1:5 \tag{15}$$

where $f(x_i)$ represents the response values, $F(x_i)_{con}$ is the constraint condition, and C_i is the penalty function.

The fitness proportional model (also known as Monte Carlo) is adopted. The set of variables in the sample is represented as a chromosomal/genetic representation. In the iterative process, 60 initial samples are generated by Latin hypercube sampling, the corresponding structure is established through finite element simulation and the response is calculated. Based on the fitness function established above, six samples with the best fitness are selected as the parents of the next generation, and the parents generate new offspring through single-point crossover. The mutation process occurs during the generation of offspring. The process of evaluation, fitness calculation, selection, and crossover would be repeated until the termination condition of the algorithm was met (after 50 generations of iteration). The algorithm is implemented based on Matlab. The specific parameters of the algorithm are summarized in Table 2.

Example application

Based on the presented method, a CBS with a diameter of 3 m and a height of 1.2 m is designed in this section. The basic parameters used for

Table 3
Physical parameters of materials.

Physical parameters	straps	interface rings and V-segments
$_E$ (MPa)	182,000	70,000
μ	0.3	0.3
ρ (kg/m^3)	7800	2700
α	1.0×10^{-5}	2.16×10^{-5}
σ_s (MPa)	1500	373

Table 4
Results of optimal design.

Optimizing parameter	Value (mm)	Optimizing parameter	Value (mm)	Optimizing parameter	Value (mm)
x_1	1	x_9	7	y_3	52
x_2	20	x_{10}	0	y_4	0
x_3	10	x_{11}	25	y_5	18
x_4	0	x_{12}	0	y_6	1
x_5	35	x_{13}	9	y_7	39
x_6	0	x_{14}	−3	y_8	0
x_7	12	y_1	60	y_9	10
x_8	−6	y_2	10	y_{10}	1

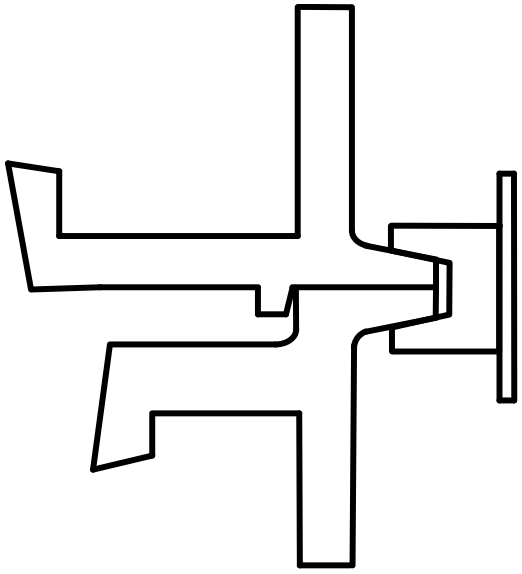

Fig. 8. Optimized configuration of CBS.

the example application are set as follows:

$$\begin{cases} EI \geq 5 \times 10^9 \text{N}\cdot\text{m}^2 \\ F_{pt} = 50\text{kN} \\ T = 1.5 \times 10^5 \text{N} \\ Q = 8 \times 10^4 \text{N} \\ M = 1.5 \times 10^5 N\cdot\text{m} \end{cases} \tag{16}$$

and safety factor is 1.5. The material parameters used in the application are shown in Table 3.

Then an optimizing program is obtained using PCL and Matlab. The coverage ratio δ defined in Eq. (2) is 0.8, and 40 V-segments are uniformly distributed along the circumferential direction. Optimization constraint conditions are taken as Eq. (17). The optimization results are shown in Table 4. The strength and stiffness of the optimized design results satisfy the constraint conditions, and the minimum mass is 140 kg.

$$\begin{cases} d\_\max \leq 2\text{mm} \\ dy \leq 0.5\text{mm} \\ dx \leq 0.1\text{mm} \end{cases} \tag{17}$$

As shown in Fig. 8, the upper stage and lower stage of the optimized configuration of CBS are asymmetric in general, which is caused by the asymmetry of the boundary conditions. In the optimal design, the boundary conditions of the upper stage are free and the lower stage is fixed. In practice, the lower end of the CBS is connected to the rocket, and its corresponding connection stiffness is larger, so the fixed boundary is added to the bottom of the lower stage. The upper end is connected to the spacecraft, and the connection is similar to a cantilever beam, so the upper boundary can be approximated as a free boundary. Based on this, the design rationality of asymmetry can be explained. However, to reduce the effects of the approximate boundary conditions, the height of CBS has increased by 100 mm.

In Fig. 9, a gap occurs at the contact lines of interface rings when applying pre-tension and total expected load. The maximum gaps at the inner edge are 0.13 mm and 0.68 mm respectively for different loads. While at the outer edge, the nodes keep contact.

Fig. 10 shows the slip and gap of the inner edge of interface rings, in which 0~1 is the process of applying pre-tension, and 1~2 is the process of applying the expected total load. A small slip occurs under different loads, and the maximum slip is less than 0.001 mm. The gap increases with the load, and the upper stage deforms in the forward direction of the Y axis, while the lower stage deforms in the opposite direction. The entire deforming curve is nonlinear, and the gap increases faster.

Verification using 3D finite element

To verify the result of 2D axisymmetric analysis, a 3D finite element model of the designed CBS was established and analyzed as shown in Fig. 11. The loading conditions between the models were ensured to be

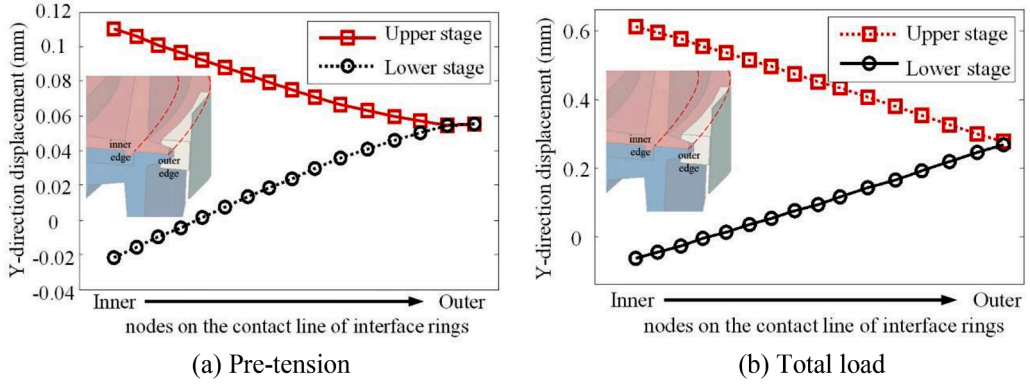

Fig. 9. Y-direction displacement of the nodes on the contact line of interface rings.

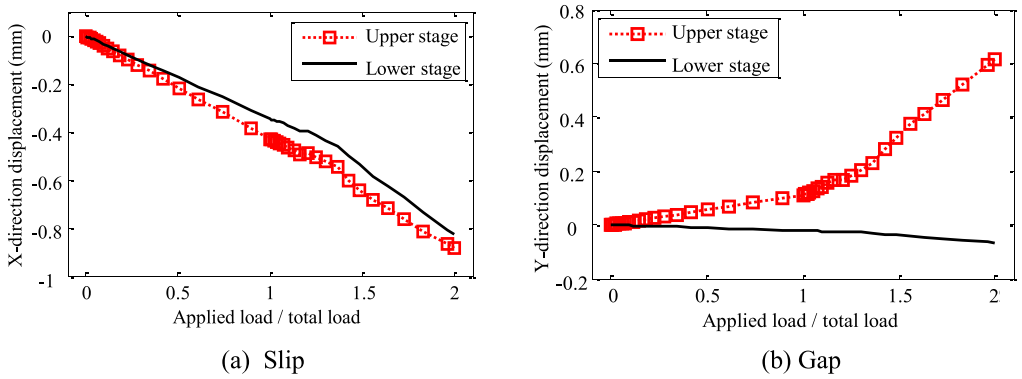

(a) Slip (b) Gap

Fig. 10. The slip and gap of the inner edge of interface rings.

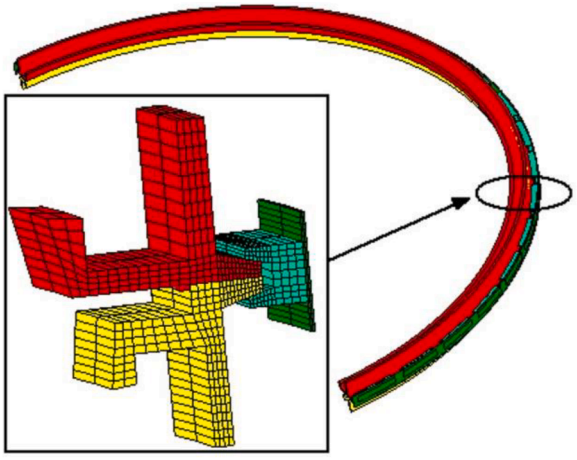

Fig. 11. 3D finite element model of CBS.

consistent, that is, the pre-tension of the strap is applied before the total load (tension, bending moment, shear) is applied. The strength characteristics were verified by the stress distribution of the 3D finite element model, and the stiffness characteristics were verified by the test data of the full-scale stiffness experiment.

Fig. 12 shows the Von-mises stress distributions obtained by the 2D axisymmetric model and 3D model, with the left figures obtained by the former model, and the right figures obtained by the later one. It can be observed from the comparison that the results obtained by the 2D axisymmetric analysis are similar to the results of the 3D model. The maximum stress values and relative error on different parts of the two models can be obtained as shown in Table 5. Among them, the maximum stress inside the V-segment needs to be converted according to the formula $\sigma_{true} = \sigma_{average}/\delta$ to obtain the true stress.

It can be seen from the data comparison that the maximum stress of the strap in the 3D model is higher than that of the 2D axisymmetric model. The relative error is caused by the processing of the connection between the strap and the V-segments. The stress distribution of the strap in the 2D model is relatively uniform. In the 3D model, the stress concentration occurs at the contact with the edge of the clamp, and the maximum stress difference is 5.3%. For the pin connection between the strap and the V-segments, the 2D model replaces the pin connection with common nodes, while the 3D model treats it as a fixed connection. Therefore, when the pre-tension is generated by the application of a temperature differential in the 2D model, the common nodes in the strap and the V-segments will bear part of the pre-tension, so that the stress of the strap in the 2D model is less. In addition, the 3D model considers the friction between the components, and the local stress concentration on the strap is due to the fact that the V-segments are not chamfered, which makes the maximum stress of the strap in the 3D model slightly higher than the actual.

The maximum stress of the two models in the V-segment and the interface rings is similar, and the relative error is less than 5%, both are generated at the outer edge of the contact surface between the upper and lower interface rings, which verifies that the 2D axisymmetric model can accurately simulate the actual situation.

Separation process and shock analysis of CBS

Different from the emphasis on the strength and stiffness of CBS in the connection stage, the separation process of each component and the shock responses of the upper stage are focused on. The explicit nonlinear analysis method is usually used for the numerical simulation of high-speed collision and impact processes, which can accurately track the mechanical behavior of high frequency and high impact amplitude during the separation process and shock of CBS. As shown in Fig. 13, finite element and pre-tension force modeling methods were present, and then the dynamic envelope of the clamp band and separation shock responses were obtained using LS-DYNA. Among them, the pull springs and the kick-off springs are in the state of elongation and contraction respectively, while the straps remain pre-tensioned before unlocking. The initial deformation of the overall structure is calculated by an implicit nonlinear static solver. The finite element modeling methods in the two stages are compared in Table 6, where t_{sep} is the CBS separation process time and t_{unlock} is the time for the pre-tension to disappear, and their values are determined according to engineering data. The contact algorithm of the penalty method and the Coulomb friction model are adopted in the established model. The incrementation is automatically calculated by the program, and the minimum time increment step is controlled by mass scaling. The accuracy of the simulation analysis has been verified by the CBS system separation experiment.

Separation process

The separation process is divided according to the position relationship of each component. First, the unlock is completed within 1 ms; Then, the separation between the components is completed within 1~10 ms, including the V-segments and the upper & lower stages; Finally, the straps and V-segments collide and move reciprocally between the cone section and the lower stage under the action of traction. During this period, the separation is considered to be successfully completed as long as the motion does not affect the normal operation of the upper stage and the satellite.

Fig. 14 shows the dynamic envelope of straps of radial displacement. It can be observed that the straps expand in the radial direction firstly, and then shrink under the pull springs. Fig. 14(b) and (c) respectively show the radial and axial displacement curves of four points on different positions. The straps impact the lower stage at 38 ms, and then slide on

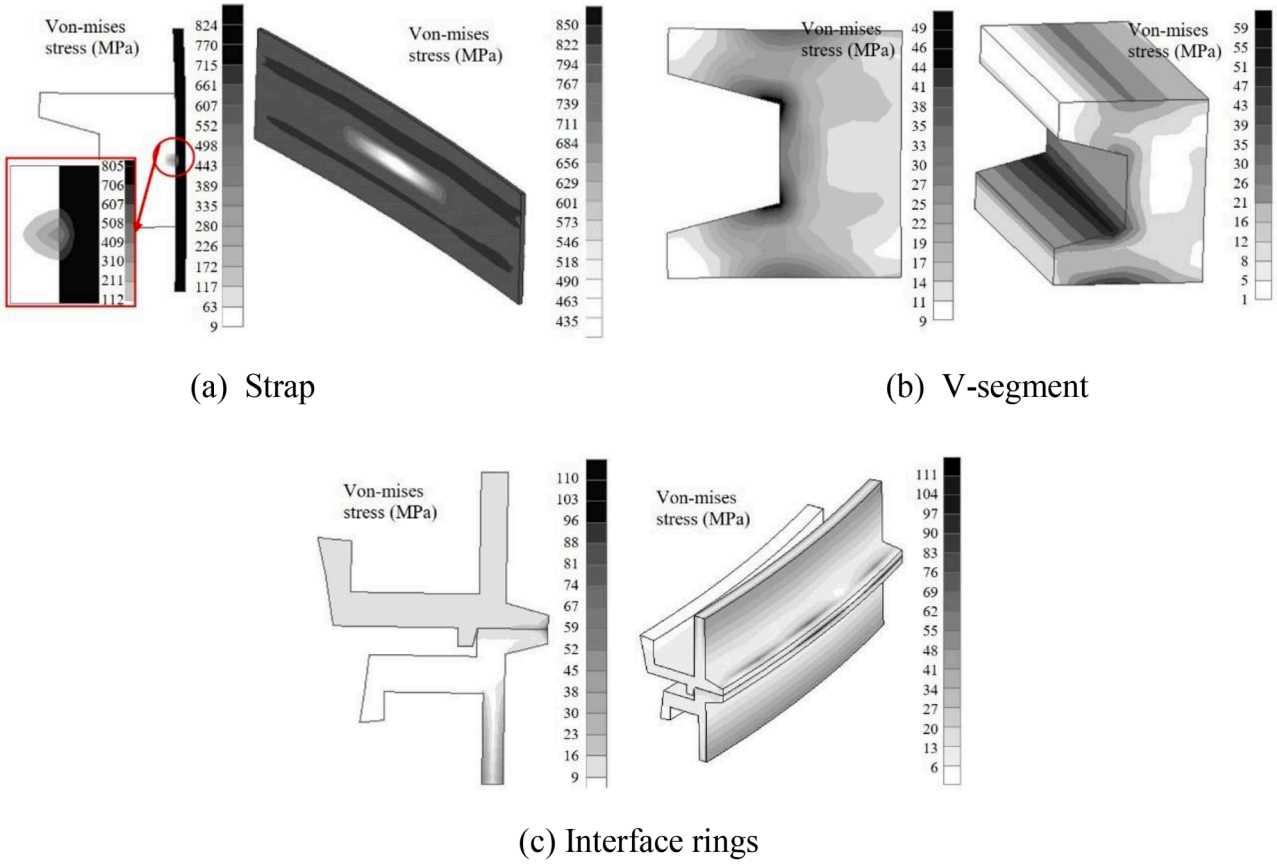

Fig. 12. Comparison of stress distributions obtained by 2D axisymmetric model and 3D model.

Table 5
Comparison of maximum stress of model components.

Part	Maximum stress in 2D model/ MPa	Maximum stress in 3D model/ MPa	error
Strap	805	850	5.3%
V-segment	61.25	59	−3.8%
Interface rings	110	111	0.9%

the lower stage for a short time. The impulse generated by the collision has a radial component, so the radial velocity increases and the axial velocity decreases, which is reflected in the change of the slope of the displacement curve. The radial displacement reaches to maximum value at 56 ms, and in the end, the straps will stop at a balanced position until the force of the pull spring equals the friction force.

Shock analysis of CBS

At the same height from the separation plane (35 mm), radial acceleration response curves are extracted at two different circumferential positions (10° and 80°), as shown in Fig. 15. The maximum acceleration of the former curve appears at 3 ms, but the latter one is at 7 ms. This

Table 6
The modeling methods in connection and separation stage.

Period	Simulation tool	Solver	Convergence criterium	Related parameters
Connection stage	MSC.Patran	MSC.Marc	Load complete	Eq. (16)
Separation stage	LS-DYNA	Explicit dynamics	Separation complete	$t_{sep} = 0.5$ s $t_{unlock} = 1$ms

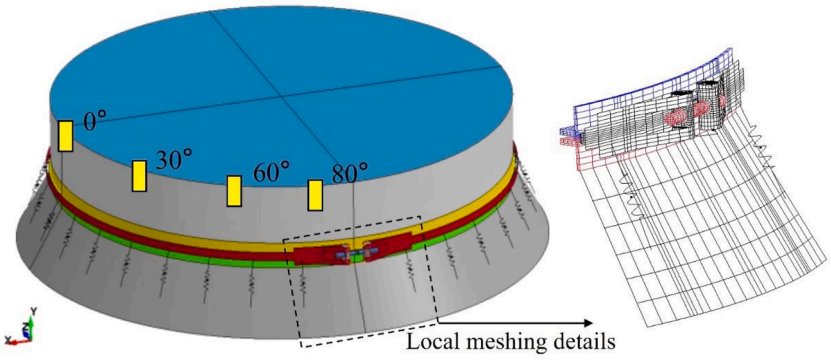

Fig. 13. Configuration of finite element model for analysis using LS-DYNA.

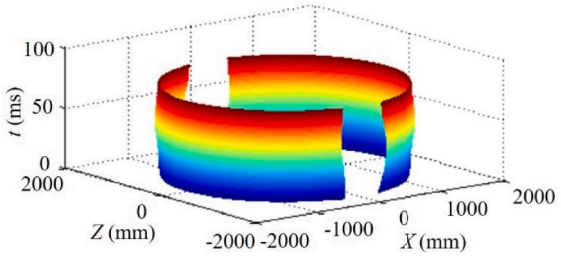

(a) The envelope of straps

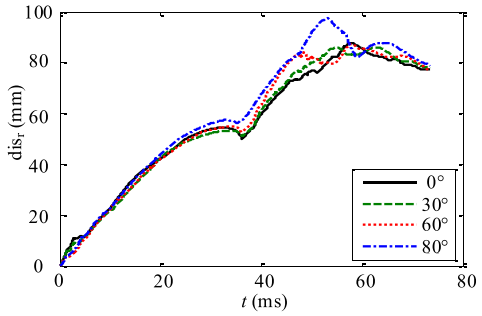

(b) Displacement in the radial direction

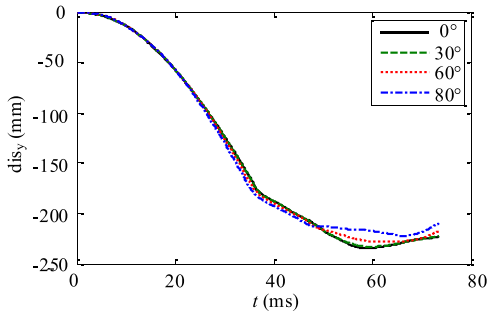

(c) Displacement in the axis direction

Fig. 14. Dynamic envelope of band and displacement response curves.

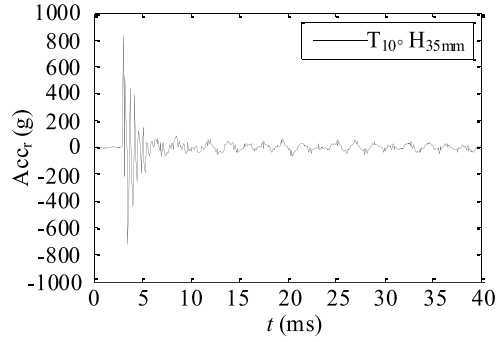

(a) 10°

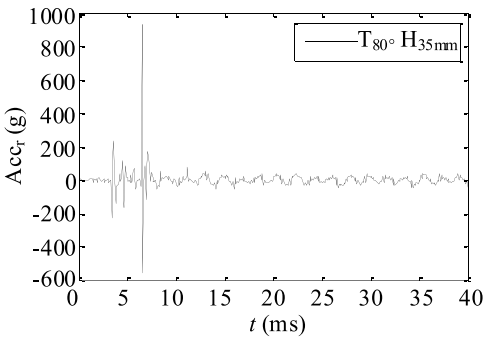

(b) 80°

Fig. 15. Acceleration response of the upper stage.

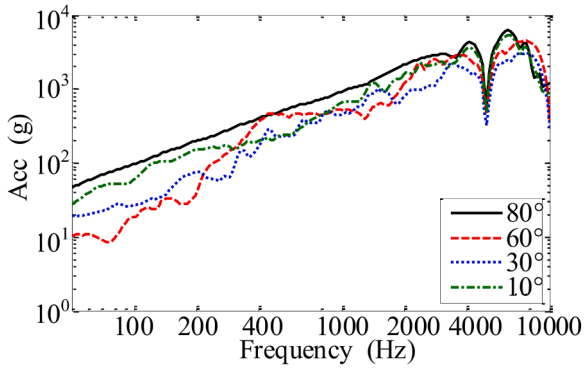

Fig. 16. Shock response spectrum of the upper stage.

asynchronous phenomenon can be explained in the separation process. After unlocking the straps, the V-segments start to detach from the interface rings. When it is about 3 ms, the upper stage receives a large impact, but the detachment of the V-segments is not synchronized. The V-segment in the middle of the strap (at 0° position) breaks away first, and its strain energy is released at one time. For the V-segment at the joint position (at 80° position), there is a sliding process along the interface rings. Part of its strain energy is released at 3 ms, and the complete detachment occurs until 7 ms. Therefore, two response peaks are reflected on the acceleration response curve.

In addition to analyzing the Response in the time domain, the Shock Response Spectrum index (SRS) is generally used to evaluate the acceleration [33–34]. The asynchronous radial acceleration response of the upper stage during unlocking is further explained by the SRS curve shown in Fig. 16. The trend of SRS curve at different positions is generally consistent. The highest shock response corresponds to the 80° position, with a maximum response of 6109 g among two distinct response peaks, corresponding to a frequency of 8192 Hz. Regardless of the position, the shock responses are of high amplitude and high

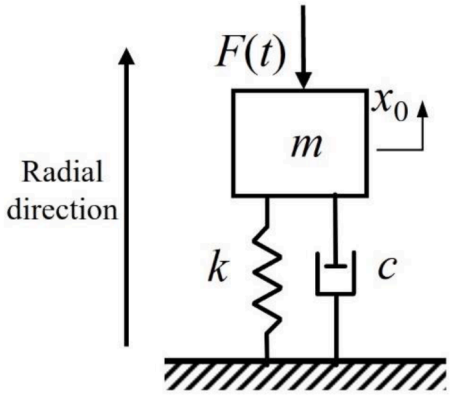

Fig. 17. Single-degree 'spring-mass' system.

frequency, which leads to some research on reducing the separation shock responses of CBS has become an important topic.

Analysis by equivalent SDOF spring-mass system

The stability problem of the satellite entering the orbit arises when the shock response is too large during the separation process of CBS. An effective way to solve this problem is to increase the release time of shocks in separation. It has been proven that, in a low-shock clamp band separation system, the shock response can be controlled at less than 400 g when the energy release time is extended by 2~5 ms [35]. Here, an explanation of time delaying for shock response is presented based on a SDOF spring-mass model with initial displacement x_0 in Fig. 17.

SDOF is a typical equivalent model for predicting the impact of satellite-rocket separation [6,9]. The motion equation of a single-degree system is given by

$$m\ddot{x} + c\dot{x} + kx = F(t) \tag{18}$$

where m, c and $k$represent mass, damping and stiffness, respectively; $F(t)$ denotes the radial force of V-segments against the upper stage; x,$\dot{x}$and $\ddot{x}$ are the radial displacement, velocity, and acceleration of the upper stage, respectively. Among them, analysis parameters in terms of the natural frequency and initial displacement are required, which are obtained based on CBS.

The radial force p in the upper stage is given by

$$\begin{aligned} 2T &= \int_0^{\pi} 2pR_{equ}\sin\theta d\theta \\ p &= \frac{T}{2R_{equ}} \end{aligned} \tag{19}$$

where R_{equ} denotes equivalent radius in the upper stage.

The external forces work W_0due to the pre-tension T is written as

$$W_0 = \pi R_{equ} p x_0 = \frac{1}{2}\pi T x_0 \tag{20}$$

After pre-tensioning of straps, the strain energy E_0 stored in the upper stage is given as

$$E_0 = \int_V \sigma d\varepsilon = \int_V E\varepsilon d\varepsilon = 2\pi R_{equ} AE \int_0^{x_0} \frac{x}{R_{\text{equ}}^2} dx = EA\pi \frac{x_0^2}{R_{\text{equ}}} \tag{21}$$

According to the conservation of energy, x_0 is obtained by

$$\begin{aligned} \frac{1}{2}\pi T x_0 &= EA\pi \frac{x_0^2}{R_{equ}} \\ x_0 &= \frac{TR_{equ}}{2EA} \end{aligned} \tag{22}$$

The separation is divided into two stages of free vibration: firstly, it can be simplified as a free vibration with delay time, and the second process is a free vibration of the upper stage. In the first stage, the time for the initial displacement x_0 to decrease to zero is increased. When T_o is assumed to be the period of free vibration without considering the delay time, and the delay time is t_d, the circular frequency of this stage is

$$\omega_1 = \frac{2\pi}{T_0 + 4t_d} \tag{23}$$

where $T_0 = \frac{1}{f_0}, f_0 = \frac{1}{2\pi}\sqrt{\frac{E}{\rho R_{equ}}}$, which is the free vibration frequency of the equivalent interface ring [6], and ρ is density. The response of displacement and acceleration are respectively:

$$x_1 = \sqrt{x_0^2 + \frac{(\dot{x}_0 + \zeta\omega_1 x_0)^2}{(1-\zeta^2)\omega_1^2}} e^{-\zeta\omega_1 t} e^{j(\omega_{1d}t + \phi_1)} \tag{24}$$

$$\ddot{x}_1 = (-\zeta\omega_1 + j\omega_{1d})^2 \sqrt{x_0^2 + \frac{(\dot{x}_0 + \zeta\omega_1 x_0)^2}{(1-\zeta^2)\omega_1^2}} e^{-\zeta\omega_1 t} e^{j(\omega_{1d}t + \phi_1)} \tag{25}$$

where, ζ is the damping ratio, $\omega_{1d} = \sqrt{1-\zeta^2}\omega_1$, $\phi_1 = \tan^{-1}\left\{\frac{\dot{x}_0 + \zeta\omega_1 x_0}{\sqrt{1-\zeta^2}\omega_1 x_0}\right\}$.

The acceleration response of the second process is the same as Eq. (25), except that $\omega_2 = 2\pi f_0$, and the initial conditions are: $x_{20} = 0, \dot{x}_{20} = \dot{x}_1(t_1)$, where $t_1 = (\pi/2 - \phi_1)/\omega_{1d}$. s an example, the parameters are $E = 70\text{GPa}$, $\rho = 2700\text{kg}/\text{m}^3$, $\zeta = 0.03$, $R_{equ} = 1.5\text{m}$,$A = 2\times10^{-4}\text{m}^2$, $T = 50\text{k}N$, and the delay time t_d is controlled from 1 to 6 ms. Fig. 18 shows the effects of the delay of release time on separation shock response. The amplitude of the maximum acceleration response is significantly reduced as delay time increases, according to Fig. 18(a). When the time exceeds 2 ms, the acceleration response is already 20%

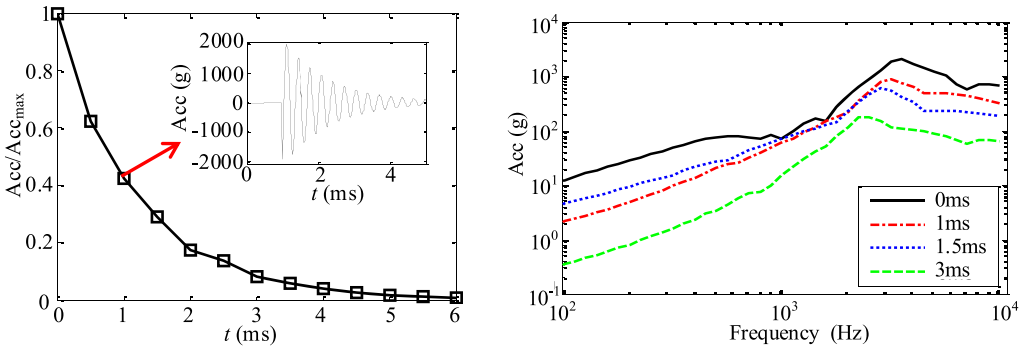

(a) The maximum acceleration response (b) Shock response spectrum

Fig. 18. Effects of the delay of release time on separation shock response.

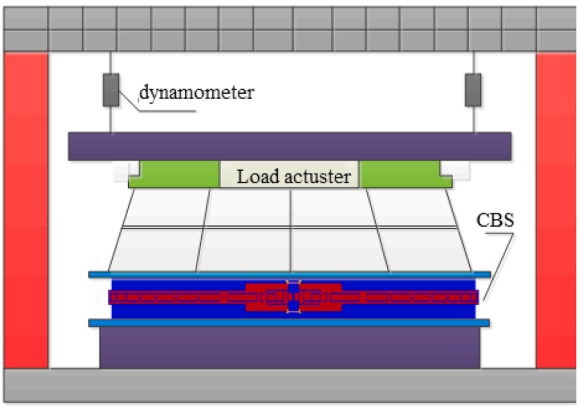

Fig. 19. Configuration of the stiffness experiment.

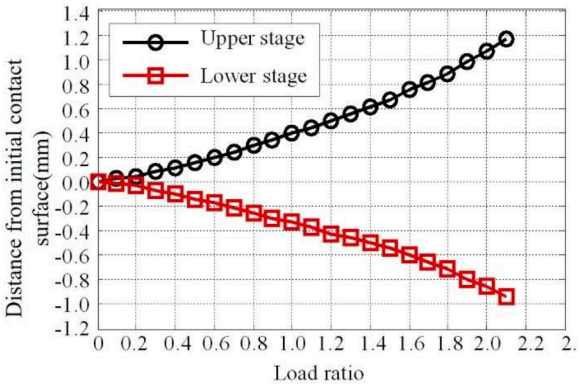

Fig. 20. The gap of the interface rings.

lower than the original. The same comparison is carried out in the experiment, and the separation shock response with a slow-release device was 19.2% lower than that with the explosive bolt. Meanwhile, the frequency corresponding to the maximum response also decreases as shown in shock response spectrum in Fig. 18(b). This result has also been verified through the experiment, the results show that the frequency corresponding to the maximum impact spectrum when the explosive bolts are used is 4794.4 Hz, while a slow-release device with a delay time of about 2.75 ms is used, the frequency corresponding to the maximum impact spectrum is 4271.5 Hz. The validity of the SDOF model is fully illustrated based on the above results.

Validation of two full-scale experiments

Stiffness experiment

The CBS designed in Section 2 is manufactured, and then the stiffness experiment is executed. The configuration of the stiffness experiment is shown in Fig. 19. The CBS is fixed on a test platform, and the pre-tension of straps is 50 kN. Experimental results show that the stiffness and strength of the CBS can meet the design requirements. Fig. 20 shows the gap of the interface rings. When the total load radio is one, a maximum gap of 0.72 mm occurs, and the simulation error is only 5.56% in Fig. 9, which indicates that the optimal design is valid.

Separation experiment

Figs. 21 and 22 show the configuration of the separation experiment and its results respectively. The motion trajectory and impact signal are respectively collected by high-speed camera and accelerometer. The acceleration response curves shown in Fig. 15 agree with Fig. 22(a) well, and the first peak value of SRS curves shown in Fig. 16 is about 4000 g, which is similar to the maximum value of Fig. 22(b). It indicates that the approach proposed in this paper can be used to solve both the simulation of the separation process and shock analysis of clamp band systems, and the error of results is small.

Since the research object of this paper is a large CBS system with a diameter of 3 m, and the pyro-technic unlocking method is adopted, the impact level is significantly higher than that of the traditional CBS system (maximum SRS value is around 1000 g). Based on the above research on impact reduction through delay time, a slow-release device is designed and the corresponding experiment is completed. The corresponding acceleration response curve and its SRS curve are shown in Fig. 23. Compared with Fig. 22(a), the concentrated large acceleration response is dispersed, indicating that the strain energy is slowly released. There are two obvious peaks in the SRS curve, which are consistent with the curve trend in Fig. 16, and the corresponding peak frequency difference is only 1.3%, which indicates that the simulation analysis method is effective. The peak of SRS curve is 919.0 g. It is shown that the slow-release device greatly reduces the shock response of separation.

Conclusions

In this paper, A data-driven optimization design method and a separation dynamics analysis method of a CBS are proposed. The efficient design of large-diameter CBS is realized by GA, and the analysis of separation shock response is verified by full-scale experiments. The major findings of this work are summarized below:

(1) An optimization method based on a GA-driven numerical finite element model is proposed. Among them, a 2D axisymmetric model with sufficient accuracy is established, which makes the

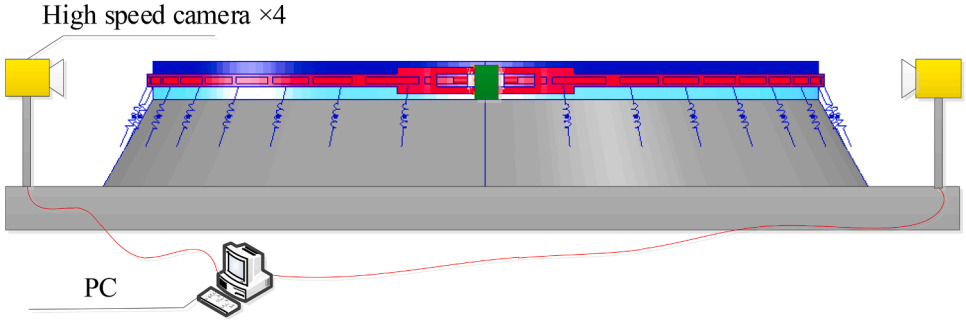

Fig. 21. Configuration of the Separation experiment.

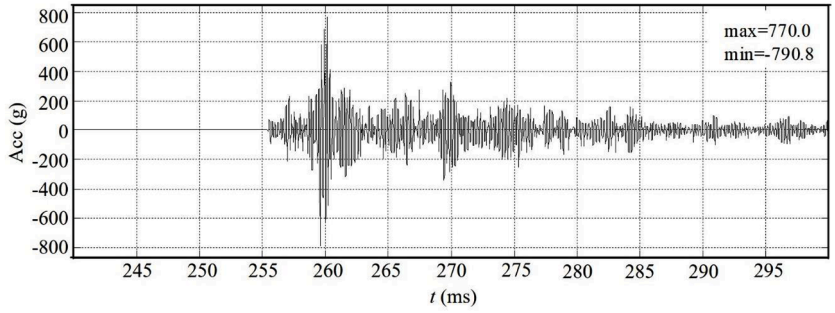

(a) Shock acceleration response curve

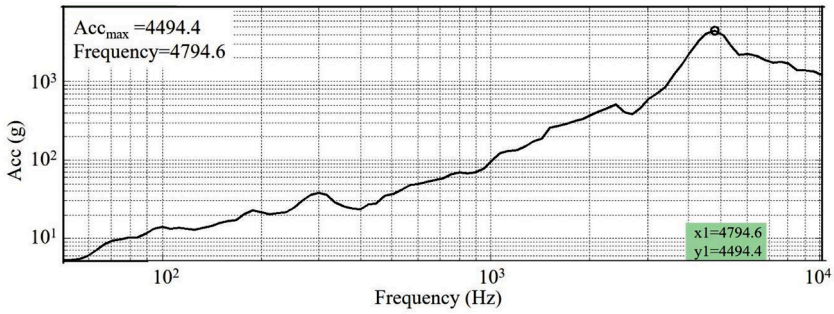

(b) Shock response spectrum curve

Fig. 22. A shock response curve obtained by separation experiment (Unlock via explosion bolts).

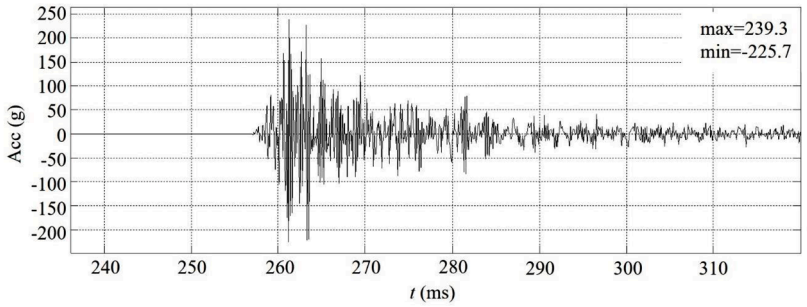

(a) Shock acceleration response curve

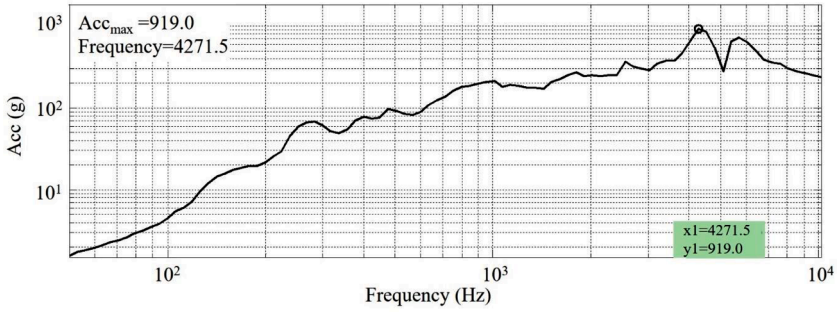

(b) Shock response spectrum curve

Fig. 23. A shock response curve obtained by separation experiment (Unlock via slow-release devices).

sample acquisition in the high-dimensional design space more rapid, thus supporting the efficient exploration of GA in the global irregular design domain.

(2) A large CBS with a diameter of 3 m is designed as a practical example of application based on the proposed optimization method. Meanwhile, a full-scale stiffness experiment is completed to verify the validity of the design.

(3) The full separation process and the associated impact response are analyzed by explicit nonlinear finite element analysis in LS-DYNA. In addition, use of a SDOF spring-mass model to provide

insight into the effect of release time delay on separation shock response. The impact response analysis and the design of the slow-release device are verified in the full-scale separation experiment.

The optimal design method can lead to more efficient and lighter CBSs for launch vehicles, improving performance. In addition, the 2D modeling techniques can enable more reliable analysis to avoid empirical over-design and reduce costs. The separation and shock analysis will help develop better pyroshock mitigation and spacecraft release devices, and further improve the reliability.

Declaration of generative AI in scientific writing

Authors did not use generative artificial intelligence (AI) and AI-assisted technologies in the writing process.

CRediT authorship contribution statement

Baoshi Yu: Conceptualization, Data curation, Formal analysis, Investigation, Methodology, Software, Writing – original draft, Writing – review & editing. **Dapeng Zhang:** Funding acquisition, Investigation, Methodology, Project administration. **Xinfeng Wu:** Conceptualization, Data curation, Software, Validation, Visualization. **Sondipon Adhikari:** Supervision, Visualization, Writing – original draft, Writing – review & editing. **Yongjun Lei:** Funding acquisition, Investigation, Project administration, Resources, Supervision, Validation.

Declaration of competing interest

The authors declare that they have no known competing financial interests or personal relationships that could have appeared to influence the work reported in this paper.

Data availability

No data was used for the research described in the article.

Acknowledgments

This research was supported by National Natural Science Foundation of China (Grant Nos. 11902348 and 11872372), Natural Science Foundation of Hunan Province, China (Grant No. 2020JJ5650), and Science Project of the National University of Defense Technology (Grant No. ZK20-27).

Supports provided by College of Aerospace Science and Engineering of National University of Defense Technology are acknowledged.

References

[1] A. Davar, R. Azarafza, S.S. Mousavi, Uncertainty analysis and reliability estimation of clamp band joints, J. Mater. Sci. Technol. 36 (2020) 1487–1502.
[2] Z.Y. Qin, S.Z. Yan, F.L. Chu, Analytical modeling of clamp band joint under external bending moment, Aerosp. Sci. Technol. 25 (2013) 45–55.
[3] Marman NASA, Clamp system design guidelines, guideline No. GD-2214. NASA Goddard Space Flight Centre, 2000.
[4] J.J. Yuan, Analysis and Design of Satellite Structures, China Astronautic Publishing House, Beijing, China, 2004, pp. p434–p478.
[5] D.T. Robert, E. Michael, Nonlinear finite element evaluation of marman clamp structural capability, in: 35th AIAA /ASME /ASCE /AHS /ASC Structures, Structural Dynamics, and Materials Conference, 1994. Conference Paper AIAA-94-1346-CP.
[6] T. Iwasa, Q. Shi, S. Ando, et al., Simplified SRS prediction method for pyroshock source of V-band clamp separation devices, in: 48th AIAA /ASME /ASCE /AHS /ASC Structures, Structural Dynamics, and Materials Conference, 2007. Conference Paper AIAA-2007-2020.
[7] J. Li, S. Yan, X. Tan, Dynamic-envelope analysis of clamp-band joint considering pyroshock of satellite Sepa-ration, J. Spacecr Rockets 51 (2014) 1390–1400.
[8] J.I. Rome, V.K. Goyal, N.E. Martino, et al., Techniques for finite element analysis of clamp band systems, in: 50th AIAA /ASME /ASCE /AHS /ASC Structures, Structural Dynamics, and Materials Conference, 2009. Conference Paper AIAA-2009-2353.
[9] J. Singaravelu, S. Sundatrsan, R.B. Nageswara, Application of fracture mechanics to specify the proof load factor for clamp band systems of launch vehicles, J. Mater. Eng. Perform. 22 (2012) 926–935.
[10] S.M. Barrans, M. Muller, Finite element prediction of the ultimate axial load capacity of V-section band clamps, J. Phys. Conf. Ser. 181 (2009) 1–9.
[11] S.M. Barrans, G. Khodabakhshi, Q. Xu, Contact pressure distribution in joints formed by V-band clamps, Adv. Mat. Res. 1016 (2014) 34–38.
[12] S. Takeuchi, J. Onoda, Estimation of separation shock of the marman clamp system by using a simple band-mass model, T Jpn. Soc. Aeronaut. S 45 (2002) 53–60.
[13] X.F. Tan, S.Z. Yan, Simplified analytical method of radial shock response of satellite-rocket separation interface, J. Mech. Eng. 46 (2010) 95–100.
[14] Z.Y. Qin, S.Z. Yan, F.L. Chu, Influence of clamp band joint on dynamic behavior of launching system in ascent flight, J. Aerosp. Eng. 228 (2012) 97–114.
[15] Z.Y. Qin, D.L. Cui, S.Z. Yan, et al., Hysteresis modeling of clamp band joint with macro-slip, Mech Syst Signal Process 66 (2016) 89–110.
[16] Z.Y. Qin, S.Z. Yan, F.L. Chu, Improved formulation for predicting the load capacity of Marman Clamps, J Spacecr Rockets 54 (2017) 395–402.
[17] Z.Y. Qin, S.Z. Yan, F.L. Chu, Dynamic analysis of clamp band joint system subjected to axial vibration, J. Sound Vib. 329 (2010) 4486–4500.
[18] Z.Y. Qin, S.Z. Yan, F.L. Chu, Finite element analysis of the clamp band joint, Appl. Math. Model. 36 (2012) 463–477.
[19] Z.Y. Qin, D.L. Cui, S.Z. Yan, et al., Application of 2D finite element model for nonlinear dynamic analysis of clamp band joint, J. Vib. Control 23 (2017) 1480–1494.
[20] H. Zhu, D.D. Li, H. Nie, X.H. Wei, Y.Z. Wei, Multiobjective optimization of a staggered-rotor octocopter design based on a surrogate model, Aerosp. Sci. Technol. 139 (2023) 108387.
[21] J.H. Lee, S.H. Yoon, C. Kim, Experimental surrogate-based design optimization of wing geometry and structure for flapping wing micro air vehicles, Aerosp. Sci. Technol. 123 (2022) 107451.
[22] H.Q. Li, Z.C. Li, Z.Z. Cheng, Z.Y. Zhou, G. Wang, B. Wang, K. Tian, A data-driven modeling and optimization framework for variable-thickness integrally stiffened shells, Aerosp. Sci. Technol. 129 (2022) 107839.
[23] L.G. Wang, Y. Liang, L.C. Long, Study on the Influence of Key Parameters of Rigid Tape on its Separation Time and Optimization Design of Tape Structure, Chinese Congress of Theoretical and Applied Mechanics, 2019. Conference Paper p2046-2053.
[24] B.S. Yu, Y.J. Lei, Z.X. Wang, et al., Lightweight design of a clamp band joint via a constrained sequential approximate optimization method in the irregular design domain, Eng. Optim (2022). Published Online.
[25] X. Guo, S.Y. Zhu, G.R. Liu, et al., Nonlinear static analysis and structural optimization of rigid clamp band connection device between launch vehicle and satellite, J. Northwest. Polytech. Univ. 38 (2020) 1122–1128.
[26] Y. Shen, W. Huang, L. Yan, et al., An automatic visible explainer of geometric knowledge for aeroshape design optimization based on SHAP, Aerosp. Sci. Technol. 131 (2022) 107993.
[27] Z.U.D. Taj, A. Bilal, M. Awais, S. Salamat, M. Abbas, A. Maqsood, Design exploration and optimization of aerodynamics and radar cross section for a fighter aircraft, Aerosp. Sci. Technol. 133 (2023) 108114.
[28] General Specification for Clamp Band Spring Satellite-Launcher Release Device, GJB, COSTIND, 2006, 2499A-2006.
[29] L. Liu, T.Q. Wang, Z.M. Gao, L.F. Zeng, X.M. Shao, Deep learning based adaptive deformation of aerodynamic shape for ducted propellers, Aerosp. Sci. Technol. 142 (2023) 108607.
[30] P.C. Wang, H. Zhu, H. Tian, G.B. Cai, Analytic target cascading with fuzzy uncertainties based on global sensitivity analysis for overall design of launch vehicle powered by hybrid rocket motor, Aerosp. Sci. Technol. 114 (2021) 106680.
[31] S. Samsam, R. Chhabra, Multi-impulse smooth trajectory design for long-range rendezvous with an orbiting target using multi-objective non-dominated sorting genetic algorithm, Aerosp. Sci. Technol. 120 (2022) 107285.
[32] C.C. Tung, Y.Y. lai, Y.Z. Chen, et al., Optimization of mechanical properties of bioinspired Voronoi structures by genetic algorithm, J. Mater. Res. Technol. 26 (2023) 3813–3829.
[33] Y.Z. Yan, Q.M. Li, A pyroshock signal characterization method based on shock-waveform dictionary, Int. J. Mech. Sci. 249 (2023) 108251.
[34] D.S. Hou, Q.M. Li, Damage boundaries on shock response spectrum based on an elastic single-degree-of-freedom structural model, Int. J. Impact Eng. 173 (2023) 104435.
[35] D. Dowen, S.S. Christiansen, A. Peffer, Development of a reusable, low-shock clamp band separation system for small spacecraft release applications, in: 9th European Space Mechanisms and Tribology Symposium, 2001. Conference Paper p191-199.